

PROPULSION-AIRFRAME INTEGRATED AERODYNAMIC PREDICTION METHOD USING FASTAR FOR SPACEPLANE CONCEPTUAL DESIGN

Kenta Tsukuda[1], Haruyuki Kato[1], Daisuke Sasaki[1],
Chihiro Fujio[2], Shun Takahashi[2], Tatsushi Isono[2], Masaru Koga[2] & Masao Takegoshi[2]

[1]Osaka Metropolitan University, Sakai, Japan
[2]Japan Aerospace Exploration Agency, Kakuda , Japan

Abstract

In this study, an integrated airframe-propulsion analysis model combining 3D Euler analysis and quasi-1D (Q1D) flow analysis was developed for application in the conceptual design of spaceplanes. The developed Q1D solver captured the overall trend of the experimental results for both ramjet and scramjet combustions. By evaluating the total thrust and pitching moment coefficients, this study demonstrated the potential of the proposed model to capture the interference effects between the airframe and the propulsion system.

Keywords: Spaceplane, Airframe-Propulsion Integration, Quasi-1D Flow, Euler

1. Introduction

Spaceplanes, anticipated as next-generation space transportation systems, are known to exhibit strong aerodynamic interaction between the airframe and the propulsion system. To properly evaluate these airframe-propulsion interference effects, an integrated analysis that considers the internal flowpaths of the propulsion system is indispensable, rather than relying solely on aerodynamic analysis of the airframe geometry.

In evaluating propulsion systems such as scramjet and ramjet engines, two- or three-dimensional reacting CFD analysis is a highly effective approach. However, due to its prohibitive computational cost, applying such high-fidelity CFD to the conceptual design phase—which involves extensive parametric studies—is impractical [1]. In contrast, utilizing low-fidelity models, typified by quasi-one-dimensional flow models, is highly reasonable from the perspective of computational efficiency. For isolated engine analysis, numerous quasi-one-dimensional flow models have already been proposed and have demonstrated good agreement with experimental data [2–4].

Nevertheless, as previously mentioned, spaceplane design demands consideration of the strong mutual interaction between the airframe and the propulsion system. Therefore, it is essential to establish an integrated analysis method that couples the airframe and the propulsion system rather than analyzing the engine in isolation. To address this, we propose a hybrid analysis model that evaluates the external flow around the airframe using a three-dimensional Euler analysis and the internal flow within the propulsion system using a quasi-one-dimensional flow model. This approach enables the evaluation of airframe-propulsion interference while minimizing the computational workload.

2. Analytical Method

2.1 Integrated Airframe-Propulsion Model

The outline of the integrated airframe-propulsion model in this study is shown in Figure 1. This model is a hybrid model that analyzes the flow around the airframe excluding the propulsor using 3D Euler analysis with an unstructured grid fluid analysis solver FaSTAR (FAST Aerodynamic Routines) [5],

https://doi.org/10.71945/icas2026_0370

and analyzes only the combustion process inside the propulsor consisting of a constant-area isolator and a diverging combustor using a quasi-1D flow model. By replacing the chemical reaction process, which causes a computational load in combustion CFD analysis, with a quasi-1D flow model that can consider cross-sectional area changes and heat transfer, the computational cost is significantly reduced.

The specific analysis procedure is as follows. First, a 3D Euler analysis (flow-through analysis) is performed on the entire aircraft including the internal engine flow path to obtain the propulsor inlet boundary values. Using the obtained propulsor inlet boundary values as inflow conditions, a quasi-1D flow analysis is performed to obtain the propulsor outlet boundary values. Next, 3D Euler analysis is performed again by giving the propulsor outlet boundary values to the grid where the propulsor inlet and outlet boundaries are set. Finally, the aerodynamic coefficients of the entire aircraft are obtained by adding the propulsor aerodynamic coefficients obtained from the quasi-1D flow analysis and the aerodynamic coefficients excluding the propulsor obtained from the analysis with propulsor boundaries.

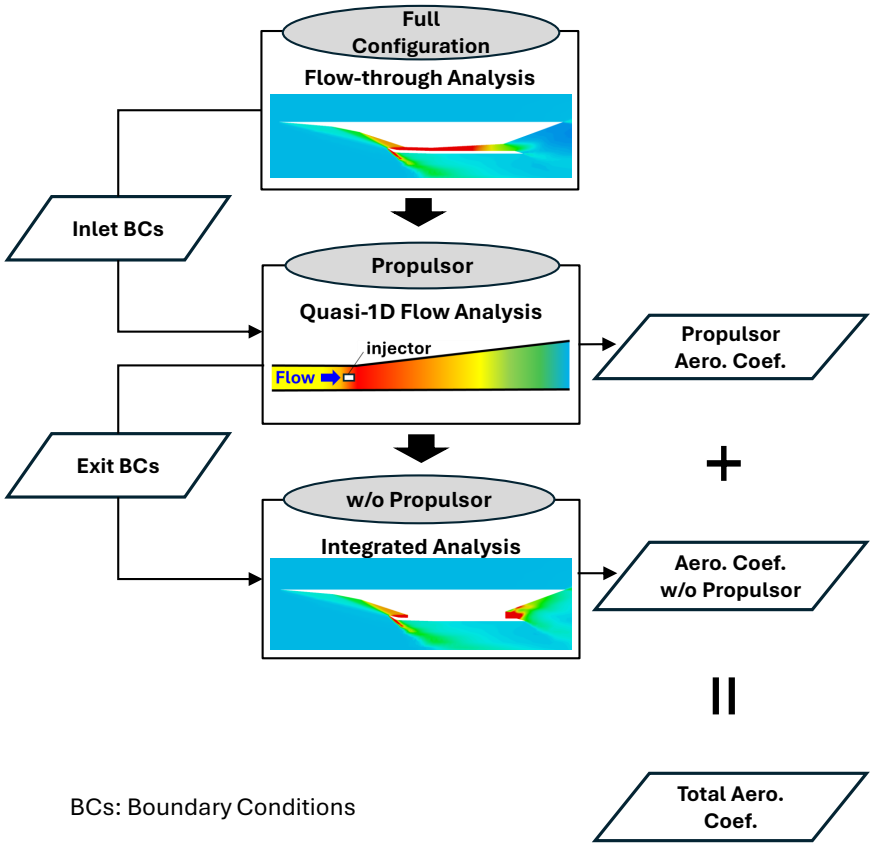


Figure 1 – Flowchart of integrated airframe-propulsion analysis.

2.2 Quasi-1D Flow Model

In this section, the numerical model constructed to analyze the combustion flow inside the dual-mode combustor is described. In this study, we emphasize the computational efficiency in the iterative calculations of the conceptual design phase and adopt a quasi-1D steady reacting flow model. The working fluid is a gas mixture consisting of multiple chemical species, and the thermodynamic properties based on a chemical reaction model using the open-source chemical kinetics library Cantera [6] are considered. The combustion reaction is determined by considering both the macroscopic mixing process of fuel and air (mixing model) and the microscopic reaction rate by a detailed chemical reaction mechanism.

Figure 2 shows the analysis flowchart of the quasi-1D flow solver. This solver implements a dual-

mode analysis function that automatically switches between scramjet mode and ramjet mode depending on the calculation conditions. First, the calculation is performed in scramjet mode based on the given mixing efficiency distribution and fuel equivalence ratio. When thermal choking is detected in the combustor, it transitions to ramjet mode. For the analysis of the ramjet mode, the method proposed by Arakawa et al. is adopted [4]. In this mode, the thermodynamic properties in the pseudo-shock wave region are calculated from the assumed maximum pressure value p_{peak}within the combustor, and the combustion calculation downstream of the injector is performed using a system of quasi-1D governing flow equations. In ramjet combustion, there is a singular solution that smoothly passes through the singular point of $M = 1$ while balancing the acceleration effect by combustion and the deceleration effect by divergence. This solver is designed to sweep and search for the singular solution while changing the maximum pressure value p_{peak}.

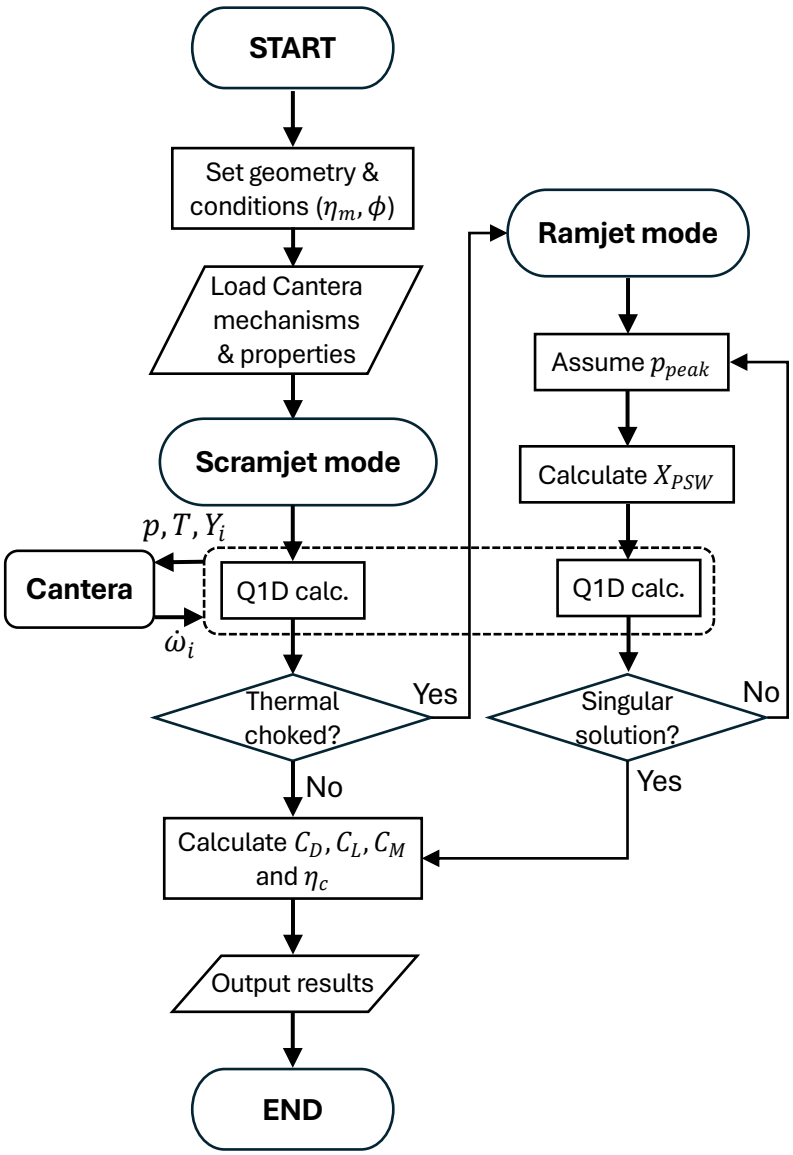


Figure 2 – Flowchart of quasi-1D flow analysis.

2.2.1 Governing Equations

The state variable vector $\boldsymbol{y}$ in this model consists of flow velocity U, density ρ, static pressure p, force and moment components F_x, F_y, M_y, boundary layer momentum thickness θ, and the mass fraction of each chemical species Y_i, and the solution is obtained by integrating the following system of governing equations in the flow direction. The law of mass conservation is described as follows,

considering the added mass of the injected fuel:

$$\frac{d\rho}{dx} = \frac{1}{UA}\left(\frac{d\dot{m}}{dx} - \rho U\frac{dA}{dx} - \rho A\frac{dU}{dx}\right) \tag{1}$$

where A is the cross-sectional area and $\dot{m}$ is the mass flow rate. The law of momentum conservation is formulated as a differential equation for flow velocity, considering wall friction loss and momentum exchange of injected fuel:

$$\begin{aligned}\frac{dU}{dx} =& \frac{1}{M^2-1}\left[\frac{U}{A}\frac{dA}{dx} - \frac{1}{\dot{m}}\frac{\gamma-1}{\gamma pA}\left(\frac{dQ_{net}}{dx}\right)\right.\\ &\left.+\frac{\gamma M^2 U}{2}\frac{4c_f}{D_h} + \frac{U}{\dot{m}}\frac{d\dot{m}}{dx}\left(1+\gamma M^2\left(1-\frac{U_{inj}\cos\beta}{U}\right)\right)\right]\end{aligned} \tag{2}$$

where M is the Mach number, c_f is the wall skin friction coefficient, D_h is the hydraulic diameter, U_{inj} is the fuel injection velocity, and β is the fuel injection angle. The energy conservation law is calculated using the partial molar enthalpy $\bar{h}_i$ including the enthalpy of formation of each species obtained from Cantera and the molar production rate $\dot{\omega}_i$:

$$\frac{dQ_{net}}{dx} = A\sum_i(-\dot{\omega}_i\bar{h}_i) - \frac{dQ_{loss}}{dx} + \frac{d\dot{m}_f}{dx}(h_{f,total} - h_{total}) \tag{3}$$

The reacting fuel flow rate $\dot{m}_f$ over a micro distance dx can be described using the spatial gradient of the mixing efficiency as follows:

$$\frac{d\dot{m}_f}{dx} = \dot{m}_{f,total}\cdot\frac{d\eta_m}{dx} \tag{4}$$

Here, the total fuel flow rate $\dot{m}_{f,total}$ is expressed as follows using the air mass flow rate entering from the propulsor inlet $\dot{m}_{air}$, the given fuel equivalence ratio ϕ, and the stoichiometric fuel-air ratio f_{stoich}:

$$\dot{m}_{f,total} = \phi f_{stoich}\dot{m}_{air} \tag{5}$$

The mixing model determining the mixing efficiency η_m is detailed in the next section. Also, the mass fraction of species Y_i follows the equation:

$$\frac{dY_i}{dx} = \frac{1}{\dot{m}}\left(\dot{\omega}_i MW_i A - Y_i\frac{d\dot{m}}{dx} + \dot{\omega}_{inj,i}\right) \tag{6}$$

To account for boundary layer development, Karman's momentum integral equation is introduced:

$$\frac{d\theta}{dx} = \frac{c_f}{2} - \left[(H+2)\frac{1}{U}\frac{dU}{dx} + \frac{1}{\rho}\frac{d\rho}{dx}\right] \tag{7}$$

where the shape factor H is defined as $H = 1.3 + 0.25M^2\gamma$.
For integrated airframe-propulsion analysis, the internal wall pressure distribution $p(x)$ is integrated in the body-fixed coordinate system to obtain the force in the x-direction:

$$\frac{dF_x}{dx} = -p\frac{dA}{dx} \tag{8}$$

Using the angle of attack of the airframe α, the propulsor drag D and lift L are calculated as follows:

$$D = F_x\cos\alpha, \quad L = -F_x\sin\alpha \tag{9}$$

2.2.2 Pseudo-Shock Wave Model

When the combustor reaches a thermal choking state due to combustion, the solver transitions to ramjet mode. At this time, the pseudo-shock wave formed in the isolator is modeled using the Waltrup-Billig correlation equation [7,8] modified by Arakawa et al. [4] to apply to the divergent combustor.

$$\frac{X_{PSW}(M_{st}^2-1)Re_{\theta,st}^{0.25}}{B\sqrt{D_{st}\theta_{st}}} = 50\left(\frac{p}{p_{st}}-1\right) + 170\left(\frac{p}{p_{st}}-1\right)^2 \tag{10}$$

Here, the subscript st indicates the state quantity at the start point of the pseudo-shock wave. X_{PSW} is the length of the pseudo-shock wave, and B is a dimensionless quantity defined as the cross-sectional area ratio between the peak pressure point and the start point of the pseudo-shock wave.

2.2.3 Mixing and Chemical Reaction Models

In this study, the fuel mixing process and the heat release process due to chemical reactions are modeled separately. The solver assumes that mixing progresses exponentially with respect to the mainstream direction distance x:

$$\eta_m(x) = \eta_{m,target}[1 - \exp(-k(x - x_{inj}))] \tag{11}$$

k is a constant that defines the arrival speed to the target value of mixing efficiency $\eta_{m,target}$. To analyze the chemical reaction process of the mixed fuel and air, a reaction mechanism using Cantera is introduced. In each calculation step, the local static pressure p, static temperature T, and mass fraction of each species are used as inputs to calculate the production rate $\dot{\omega}_i$ for each chemical species. For hydrogen fuel, the reaction mechanism of 9 species and 24 reactions proposed by Zettervall [9] is adopted. In addition, the combustion efficiency η_c is defined by the following equation:

$$\eta_c(x) = \frac{m_{O_{2,a}} - m_{O_2}(x)}{m_{O_{2,a}}\phi'} \quad \text{where} \quad \phi' = \begin{cases} \phi & \phi \leq 1 \\ 1 & \phi > 1 \end{cases} \tag{12}$$

Here, $m_{O_{2,a}}$ is the mass of oxygen flowing into the propulsor, and $m_{O_2}(x)$ is the mass of oxygen remaining locally.

2.2.4 Friction and Heat Transfer Models

To evaluate the friction and heat losses on the propulsor walls, the following model considering compressibility is introduced. The reference temperature method based on the theory of Van Driest et al. is adopted to calculate the wall skin friction coefficient. The reference temperature T^* is determined by Eckert's reference temperature from the mainstream static temperature T, wall temperature T_w, and adiabatic wall temperature T_{aw}:

$$T^* = 0.5T + 0.5T_w + 0.22(T_{aw} - T) \tag{13}$$

Here, T_{aw} is defined as:

$$T_{aw} = T\left(1 + r\frac{\gamma - 1}{2}M^2\right) \tag{14}$$

Using the density ρ^* and viscosity coefficient μ^* at the reference temperature T^*, and the momentum thickness θ, the reference Reynolds number Re^*_θ is calculated:

$$Re^*_\theta = \frac{\rho^* U \theta}{\mu^*} \tag{15}$$

The friction coefficient at the reference state is calculated based on the empirical formula for a turbulent boundary layer on a smooth flat plate:

$$c^*_f = \frac{0.026}{(Re^*_\theta)^{0.25}} \tag{16}$$

The final friction coefficient is expressed as follows using the ratio of the density at the reference temperature to the mainstream density:

$$c_f = c^*_f\left(\frac{\rho^*}{\rho}\right) \tag{17}$$

Heat loss to the wall is calculated by the following equation:

$$\frac{dQ_{loss}}{dx} = \rho U c_p St(T_{aw} - T_w) \tag{18}$$

The Stanton number St is calculated using the following equation which extends Reynolds analogy with the friction coefficient:

$$St = \frac{c_f}{2}Pr^{-2/3} \tag{19}$$

Here, Pr is the Prandtl number, which is sequentially calculated from local composition and temperature by Cantera.

2.2.5 Radical Source Model

Specifically targeting only those conditions where the fuel fails to reach its auto-ignition temperature during the compression process, this study adopts a radical source model to intentionally accelerate combustion. It has been experimentally demonstrated that the presence of trace radicals promotes ignition in supersonic flows where the mean static temperature is below the auto-ignition threshold. McGuire [10] and Lorrain et al. [11] elucidated the 'radical-farming' mechanism—where a trace amount of initial radicals generated in shock-wave interaction regions drastically accelerates downstream combustion reactions—through detailed chemical kinetics analysis and shock tunnel experiments, demonstrating that supersonic ignition is highly sensitive to the initial radical concentration. Furthermore, forcing the addition of radical species into a flow field to promote combustion in CFD analysis is an effective numerical experimentation approach. Mattick and Frankel [12] conducted numerical simulations by adding trace radicals at specified ratios to the inlet boundary conditions of a supersonic combustor, showing that a solver incorporating a detailed reaction mechanism can predict the reduction in ignition distance caused by radical addition. Based on these findings, the radical source model in this study employs a method that forcibly converts a portion of the gas composition into intermediate species at a specified ratio at designated radical source locations within the computational domain.

2.2.6 Numerical Method

In this study, a space-marching method is adopted to obtain the solution downstream, using the conditions at the isolator inlet as initial values. The solve_ivp function implemented in the scientific computing library SciPy in Python is used for the numerical calculation. The numerical integration solver using the Backward Differentiation Formula (BDF) is adopted in this solver.

2.3 Analysis Target

Figure 3 shows the analysis target. This configuration has an internal engine flow path assuming the installation of a propulsion system. Figure 4 shows the appearance of the propulsion system internal flow path shape, which is the target of the quasi-1D flow analysis.

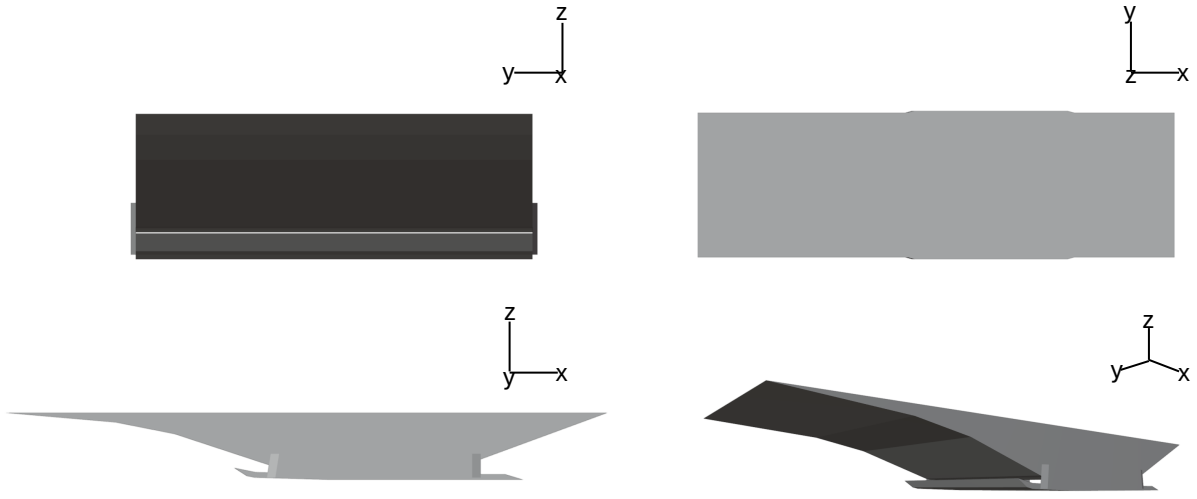


Figure 3 – Vehicle configuration. [13-15]

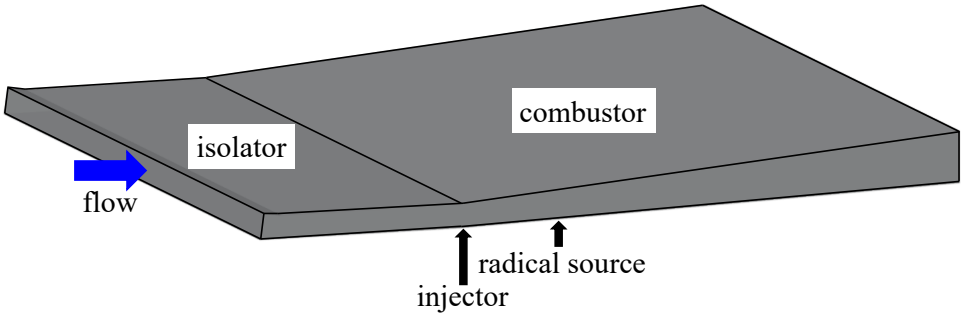


Figure 4 – Internal flow path of propulsion system.

2.4 Computational Grid

For grid generation, HexaGrid, an automated hexahedron-based mesh generation software, was used to generate an integrated analysis grid in which the propulsor inlet and outlet boundaries were placed at the inlet and outlet of the propulsor along with a flow-through grid. Figures 5 and 6 show the grid diagrams in the central cross-section viewed from the side of the airframe. Grid convergence was confirmed by the grid sensitivity analysis shown in Table 1, and a medium grid with approximately 3.9 million cells is used.

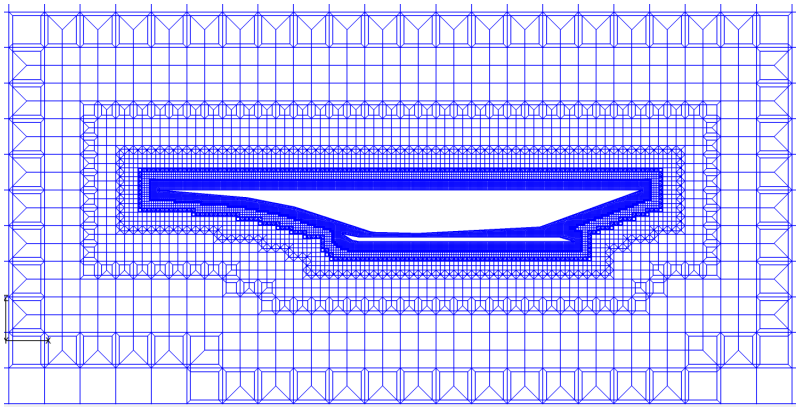


Figure 5 – Flow-through grid.

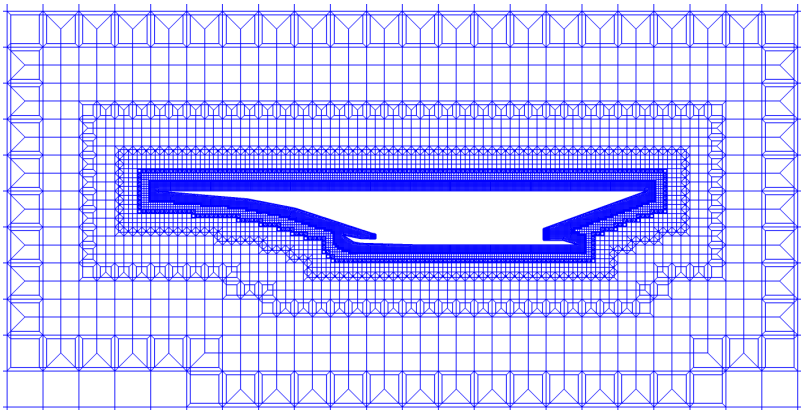


Figure 6 – Integrated analysis grid.

Table 1 – Results of grid sensitivity analysis.

	Number of Cells	Drag Coefficient C_D	Relative Error [%]
coarse	$2,213,985$	0.0279	7.88
medium	$3,885,678$	0.0259	0.07
fine	$11,987,691$	0.0259	-
	Number of Cells	Lift Coefficient C_L	Relative Error [%]
coarse	$2,213,985$	0.0591	9.58
medium	$3,885,678$	0.0538	0.27
fine	$11,987,691$	0.0539	-

2.5 Freestream Conditions

The flight Mach numbers are set to Mach 5 and 6, assuming operations of ramjet and scramjet engines. The static pressure is 2857 Pa and the static temperature is 220.8 K. The angle of attack is $-10^\circ \leq \alpha \leq 10^\circ$.

2.6 Boundary Conditions

The propulsor inlet boundary is set as a free-outflow boundary condition, and the propulsor outlet boundary is set as a fixed-inflow condition with specified velocity, static temperature, and static pressure.

3. Analysis Results

3.1 Validity of the Quasi-1D Flow Model

3.1.1 Validity of the Scramjet Mode

To verify the validity of the developed quasi-1D flow solver in scramjet mode, a comparison was made with the experimental results of the HyShot II flight test conducted by the University of Queensland [16]. As shown in Figure 7, the combustor geometry targeted for verification consists of a constant cross-section duct followed by a diverging duct. The diverging section expands by 12° on the upper wall only. Fuel was injected from four circular injection holes (diameter 2 mm) placed on the bottom surface 58 mm downstream of the combustor inlet. In this verification, conditions with fuel injection (Fuel-on) and without fuel injection (Fuel-off) were targeted. Table 2 summarizes these conditions. Figure 8 shows the comparison between the calculation results by the solver and the experimental data. For Fuel-off, it was confirmed that the solver captured the experimental results very well. For Fuel-on, while the peak pressure was reproduced well, an error of up to about 18% was observed in the region of $0.1 < x < 0.2$ m. This is considered to be because the solver predicted the fuel ignition point further downstream than in reality. In the experiment, it is inferred from the pressure distribution that combustion starts around 0.1 m, but the solver predicted that combustion starts around 0.17 m. In reality, fuel diffusing into the boundary layer near the wall may have ignited early due to longer residence time and higher static temperature than the mainstream, functioning as a flame-holding source. When obtaining the Fuel-on results, a parametric study of mixing parameters was conducted, yielding $\eta_{m,target} = 0.85$ and $k = 17.0$.

Table 2 – HyShot II experimental conditions used for verification

	Fuel-off	Fuel-on
Flight Mach Number	7.938	7.831
Angle of Attack [$^\circ$]	-5.081	5.540
Inlet Mach Number	2.6	2.563
Inlet Static Temperature [K]	1306.4	1328.2
Inlet Static Pressure [kPa]	50.53	40.994
Fuel Equivalence Ratio	0.0	0.3419

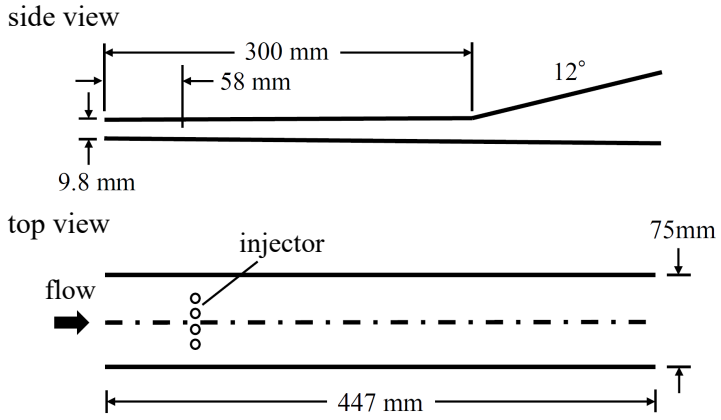


Figure 7 – Schematic diagram of the experimental HyShot II combustion duct from [16].

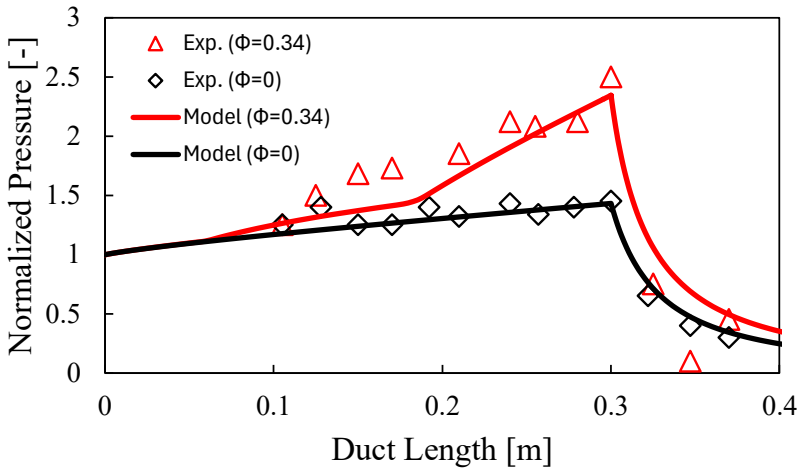


Figure 8 – Comparison of pressure distribution with experimental results from [16].

3.1.2 Validity of the Ramjet Mode

To verify the validity of the developed quasi-1D flow solver in ramjet mode, a comparison was made with the results of a dual-mode combustion experiment conducted at JAXA Kakuda Space Center [4]. The combustor geometry targeted for verification consists of a constant cross-section duct and a subsequent diverging duct, as shown in Figure 9. The diverging section expands by 3° on one side wall only. Fuel was injected from four circular injection holes (diameter 3 mm) placed on the side wall 75 mm downstream of the diverging duct inlet. In this experiment, scramjet combustion was observed at an equivalence ratio of $\phi = 0.57$, and ramjet combustion was observed at conditions exceeding $\phi = 0.85$. In this verification, Fuel-off and the experimental results of $\phi = 0.98$ and $\phi = 1.12$, where ramjet combustion was confirmed, were adopted for comparison. These experimental conditions are an inlet Mach number of 2.5, an inlet total pressure of 0.55 MPa, and an inlet total temperature of 2200 K. Figure 10 shows the comparison between the calculation results by the solver and the experimental data. In the experiment, separation near the combustor exit and the accompanying pressure rise were observed due to the pressure inside the combustor being too low compared to atmospheric pressure. Therefore, in this verification, the results for $x < 300$ mm, where the influence of separation is considered negligible, were adopted. In Fuel-off, it was confirmed that the solver captured the experimental results well. In Fuel-on, the analysis matching the fuel injection location with the experiment predicted the pressure peak point further downstream compared to the experimental values, so the analysis results in Figure 10 are those where the fuel injection position was set to the 0 mm point. Similar to HyShot II, there is a possibility that fuel diffusing into the boundary layer near the wall ignited early and combustion expanded in this experiment as well. In comparison with experi-

mental values, results predicting the start position of the pseudo-shock wave further upstream were obtained. It predicted the location about 27 mm upstream for $\phi = 1.12$ and about 150 mm upstream for $\phi = 0.98$. On the other hand, good agreement was confirmed in the section $x > 200$ mm.

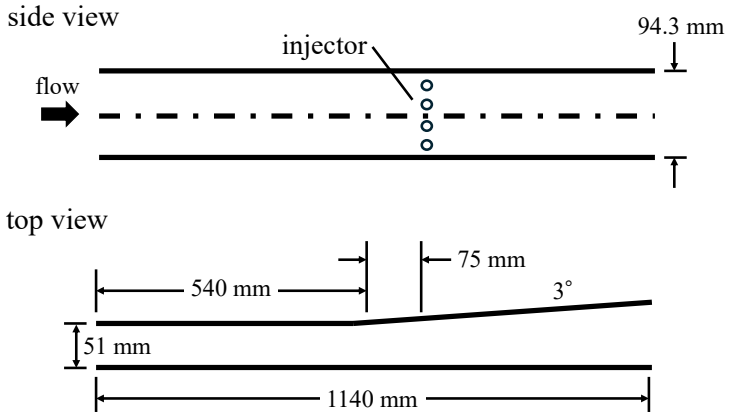


Figure 9 – Schematic diagram of the experimental combustion duct from [4].

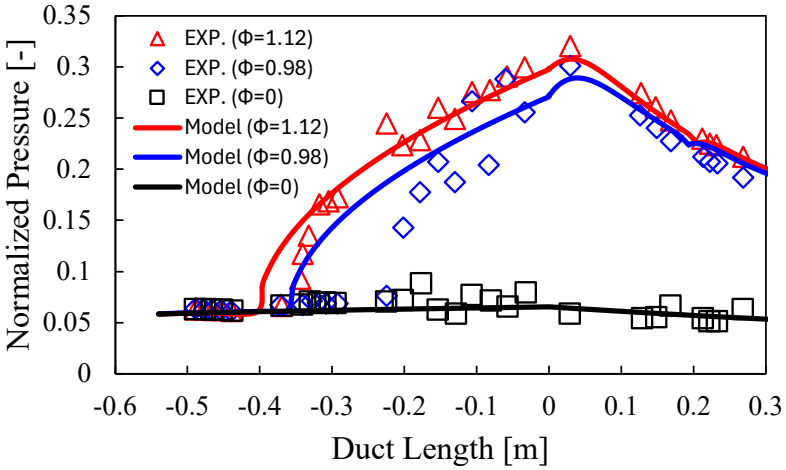


Figure 10 – Comparison of pressure distribution with experimental results from [4].

3.2 Analysis of Dual-Mode Propulsion System

Using the propulsor geometry shown in Figure 4 and the isolator inlet physical property values obtained from the flow-through analysis, a quasi-1D flow analysis inside the dual-mode propulsor was conducted. The fuel was hydrogen, the fuel equivalence ratio was set to $\phi = 0.2, 0.3, 0.4$, and the mixing efficiency was given by $\eta_{m,target} = 0.5$ and $k = 1.4$. Since the auto-ignition temperature of hydrogen fuel was not reached under these analysis conditions, the igniter model was applied. Combustion was promoted by converting hydrogen and oxygen molecules corresponding to 5.0% of the constituent gas into radicals. The propulsor thrust coefficients for each fuel equivalence ratio at flight Mach numbers of 6 and 5 are shown in Figures 11 and 12. For the analysis at $M = 6.0$, scramjet mode results were obtained under all fuel equivalence ratio and angle of attack conditions. In the scramjet mode, except for a part of the negative angle of attack region, a linear increase in the propulsor thrust coefficient was confirmed. In the negative angle of attack region, due to a lack of static temperature caused by insufficient compression at the inlet, combustion could not be sustained and expanded after ignition, resulting in an evaluation of a combustion efficiency of $0.1 - 0.2$ at the combustor exit. It is considered that sufficient thrust could not be generated as a result, breaking the linearity of the scramjet mode. The same can be said for the results at $M = 5.0$, but the most significant difference from the results

at $M = 6.0$ is that a transition to ramjet mode was confirmed at $\phi = 0.4$, $\alpha = 10^\circ$. A nonlinear increase in the propulsor thrust coefficient associated with the transition to ramjet mode was confirmed.

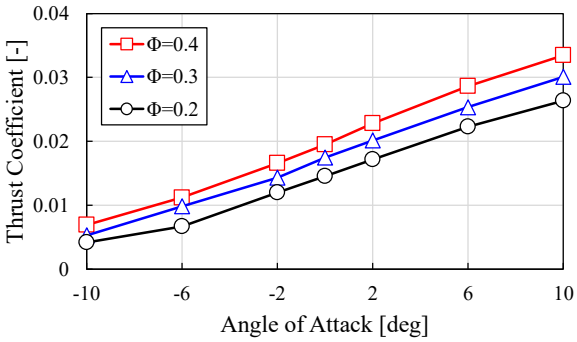


Figure 11 – Propulsor thrust coefficient ($M = 6.0$).

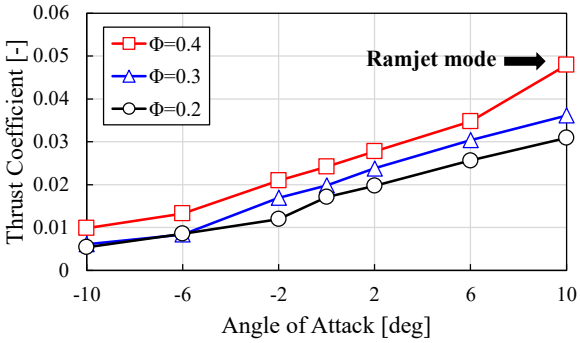


Figure 12 – Propulsor thrust coefficient ($M = 5.0$).

3.3 Integrated Airframe-Propulsion Analysis

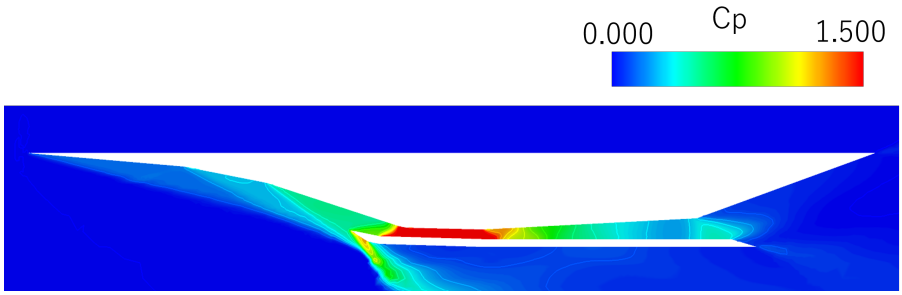
In this section, the results of integrating the analysis results from the previous section with the analysis results (3D Euler analysis) where the combustor exit physical properties obtained from the previous section were given to the propulsor exit are presented. Figure 13 displays the C_p contours at $M = 5.0$ and $\alpha = 10^\circ$ for the flow-through analysis without the integrated model and the integrated analyses across various fuel equivalence ratios. The simulations yielded scramjet combustion at $\phi = 0.2$ and ramjet combustion at $\phi = 0.4$. These comparisons reveal a high-pressure region near the combustor exit in the integrated analyses, indicating its interaction with the aft-body nozzle exhaust. We next present the total vehicle aerodynamic coefficients, which incorporate these nozzle-exhaust interactions and the internal propulsion flow effects. The total aircraft thrust coefficients and pitching moment coefficients for each fuel equivalence ratio at flight Mach numbers of 6 and 5 are shown in Figures 14, 15, 16, and 17, respectively. In the results at $M = 6.0$, surplus thrust was confirmed in the angle of attack range of approximately -2° to 2° for $\phi = 0.2$, and -7° to 5° for $\phi = 0.4$. In the results at $M = 5.0$, surplus thrust was confirmed in the angle of attack range of approximately -1° to 2° for $\phi = 0.2$, and -7° to 5° for $\phi = 0.4$. As for the pitching moment coefficient, a slight decrease was observed with the increase in the fuel equivalence ratio. This is because the exhaust jet interfered with the nozzle section at the rear of the airframe, generating a nose-down pitching moment component.

4. Conclusion

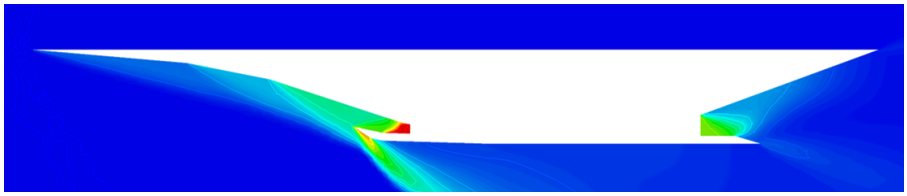
In this study, aiming at application to the conceptual design of spaceplanes, an integrated airframe-propulsion analysis model utilizing 3D Euler analysis and quasi-1D fluid analysis was developed. The developed quasi-1D solver generally reproduced experimental values well in both ramjet and scramjet modes. Furthermore, a transition to ramjet mode was confirmed under specific operating conditions, and nonlinear behavior was observed in the thrust increase on the combustor inner wall associated with this. Through the evaluation of the total aircraft thrust coefficient and pitching moment coefficient using this model, the potential to capture the interference effects between the airframe and the propulsion system was demonstrated.

5. Contact Author Information

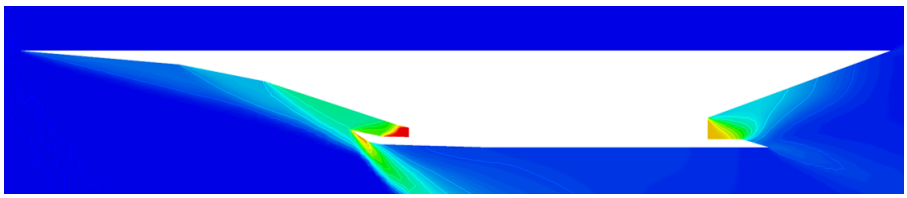
Daisuke Sasaki Department of Aerospace Engineering, Osaka Metropolitan University
1-1 Gakuencho, Naka-ku, Sakai, Osaka 599-8531, Japan
Phone: +81-72-254-9236
E-mail: daisuke.sasaki@omu.ac.jp



(a) $\phi = 0$ (flow-through)



(b) $\phi = 0.2$ (scramjet mode)



(c) $\phi = 0.4$ (ramjet mode)

Figure 13 – C_p contours ($M = 5.0, \alpha = 10°$).

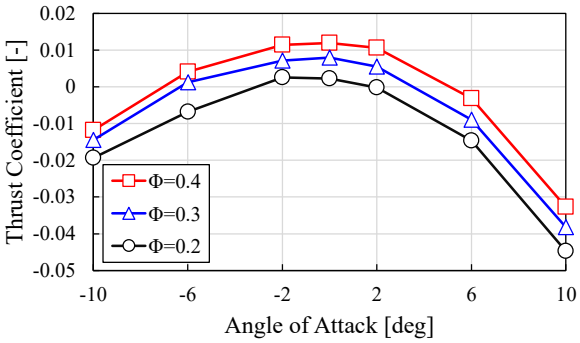


Figure 14 – Thrust coefficient ($M = 6.0$).

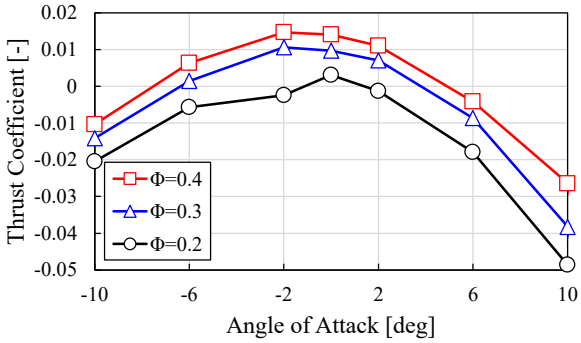


Figure 15 – Thrust coefficient ($M = 5.0$).

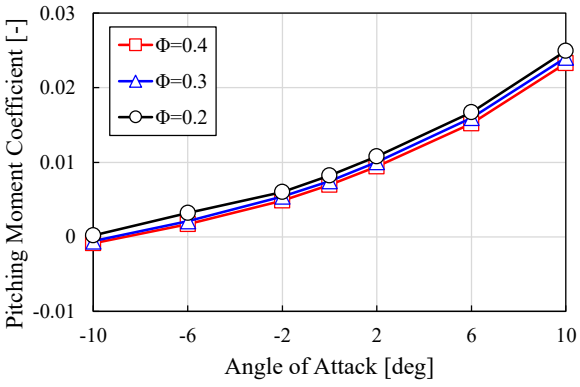


Figure 16 – Pitching moment coefficient ($M = 6.0$).

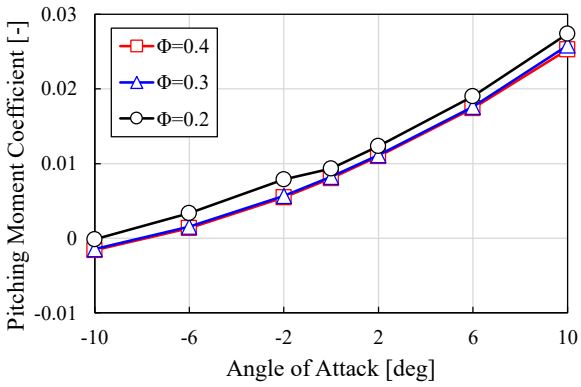


Figure 17 – Pitching moment coefficient ($M = 5.0$).

6. Copyright Statement

The authors confirm that they, and/or their company or organization, hold copyright on all of the original material included in this paper. The authors also confirm that they have obtained permission, from the copyright holder of any third party material included in this paper, to publish it as part of their paper. The authors confirm that they give permission, or have obtained permission from the copyright holder of this paper, for the publication and distribution of this paper as part of the ICAS proceedings or as individual off-prints from the proceedings.

Acknowledgment

In conducting this study, we received assistance from Mr. Koichiro Tani, Mr. Toshihiko Munakata, Mr. Taku Inoue, Mr. Masaaki Fukui, Mr. Masahiro Takahashi, Dr. Kan Kobayashi, and Dr. Sadatake Tomioka of the Japan aerospace exploration agency (JAXA) in the preparation of numerical data and in trials. We used JAXA Supercomputer System JSS3 for executing the numerical calculations.

References

[1] Bowcutt K G. Multidisciplinary Optimization of Airbreathing Hypersonic Vehicles. *Journal of Propulsion and Power*, Vol. 17, No. 6, pp. 1184–1190, 2001.

[2] Birzer C and Doolan C J. Quasi-One-Dimensional Model of Hydrogen-Fueled Scramjet Combustors. *Journal of Propulsion and Power*, Vol. 25, No. 6, pp. 1220–1226, 2009.

[3] Tian L, Chen L H, Chen Q, Li F and Chang X Y. Quasi-One-Dimensional Multimodes Analysis for Dual-Mode Scramjet. *Journal of Propulsion and Power*, Vol. 30, No. 6, pp. 1546–1555, 2014.

[4] Arakawa T, Nishiguchi H, Kobayashi K and Tomioka S. Quasi-One-Dimensional Prediction during Ramjet-mode Operation in Diverging Dual-mode Combustors. *Transactions of the JSASS*, Vol. 63, No. 6, pp. 272–280, 2020.

[5] Hashimoto A, Murakami K, Aoyama T, Hishida M, Sakashita M and Lahur P. Development of Fast Unstructured-Grid Flow Solver FaSTAR. *Journal of the Japan Society for Aeronautical and Space Sciences*, Vol. 63, No. 3, pp. 96–105, 2015. (in Japanese)

[6] Goodwin D G, Speth R L, Moffat H K and Weber B W. Cantera: An Object-oriented Software Toolkit for Chemical Kinetics, Thermodynamics, and Transport Processes. *Zenodo*, 2021.

[7] Waltrup P J and Billig F S. Structure of Shock Waves in Cylindrical Ducts. *AIAA Journal*, Vol. 11, No. 10, pp. 1404–1408, 1973.

[8] Billig F S. Research on Supersonic Combustion. *Journal of Propulsion and Power*, Vol. 9, No. 4, pp. 499–514, 1993.

[9] Zettervall N. Reaction Mechanism for Hydrogen-Air Combustion. *FOI Report*, FOI-D–1153–SE, 2021.

[10] McGuire J R. Ignition Enhancement for Scramjet Combustion. Ph.D. thesis, Department of Mechanical Engineering, The University of New South Wales, 2007.

[11] Lorrain P, Brieschenk S, Capra B R and Boyce R R. A Detailed Investigation of Nominally 2-D Radical-Farming Scramjet Combustion. *18th AIAA/3AF International Space Planes and Hypersonic Systems and Technologies Conference*, AIAA Paper 2012-5812, 2012.

[12] Mattick S J and Frankel S H. Numerical Modeling of Supersonic Combustion: Validation and Vitiation Studies Using FLUENT. *41st AIAA/ASME/SAE/ASEE Joint Propulsion Conference and Exhibit*, AIAA Paper 2005-4287, 2005.

[13] Takahashi M, Isono T, Tani K and Tomioka S. Design Study of a 2-dimensional Scramjet Inlet Operating over a Wide Range of Mach Numbers. *Proc 4th International Conference on High-Speed Vehicle Science Technology (HiSST)*, HISST-2025-0229, 2025.

[14] Tomioka S, Takegoshi M, Takahashi M, Taguchi H, Sato T, Nakaya S, Matsuo A, Kasahara J and Hayakawa A. Status of research activity titled as ground test validation of engine design method with wide operation range. *Proc 69th Space Sciences and Technology Conference*, Sapporo, Japan, 2025. (in Japanese)

[15] Takahashi M, Kobayashi K and Tomioka S. Design study of a scramjet combustor operating over a wide range of Mach numbers. *Proc 69th Space Sciences and Technology Conference*, Sapporo, Japan, 2025. (in Japanese)

[16] Hass N E, Smart M K and Paull A. Flight Data Analysis of HyShot 2. *Proc 13th AIAA/CIRA International Space Planes and Hypersonic Systems and Technologies Conference*, AIAA Paper 2005-3254, 2005.